

Modeling the optical spectrum of Romano’s star [★]

O. Maryeva ^{1†} and P. Abolmasov ²

¹*Stavropol State University, Pushkina str., 1, Stavropol, 355009, Russia*

²*Sternberg Astronomical Institute, Moscow State University, Universitetsky pr., 13, Moscow, 119992, Russia*

Accepted – . Received – ; in original form –

ABSTRACT

We consider the Luminous Blue Variable (LBV) star V532 in M33, also known as Romano’s star, in two different spectral states: in the optical minimum of 2007/2008 and during a local brightening in 2005. Optical spectra of low and moderate resolution are modeled using the non-LTE model atmosphere code CMFGEN. All the observed properties of the object in the minimum are well described by a late WN star model with a relatively high hydrogen abundance ($H/He = 1.9$), while the spectrum during the outburst corresponds to the spectral class WN11 and is similar to the spectrum of P Cyg. The atmosphere is enriched in nitrogen by about a factor of 6 in both states. Most of the heavy element abundances are consistent with the chemical composition of M33. Bolometric luminosity is shown to vary between the two states by a factor of ~ 1.5 . This makes V532 one more example of a luminous blue variable that shows variations of its bolometric luminosity during an outburst.

Key words: galaxies: individual: M33 – stars: Wolf-Rayet – stars: supergiants – stars: individual: Romano’s star (M33)

1 INTRODUCTION

Luminous Blue Variables (LBVs) are rare objects of very high luminosity ($\sim 10^6 L_\odot$) and mass loss rates (typically $10^{-5} M_\odot \text{yr}^{-1}$, up to $10^{-4} M_\odot \text{yr}^{-1}$), exhibiting strong irregular photometric and spectral variability (Conti 1984; Humphreys & Davidson 1994). They are generally believed to be a relatively short evolutionary stage in the life of a massive star, marking the transition from the Main Sequence toward Wolf-Rayet (WR) stars (Humphreys & Davidson 1994; Smith, Crowther & Prinja 1994; Maeder & Meynet 2000). Significant part of the stellar mass is lost during this stage forming massive circumstellar nebulae (Nota et al. 1995; Weis 2001) like the spectacular Homunculus surrounding η Car (Smith et al. 2003). However, recent investigations of the light curves of a few supernovae (SN2006gy, 2006tf, SN2005gl) indicate that their progenitors underwent LBV-like eruptions (Smith & McCray 2007; Smith et al. 2008; Gal-Yam & Leonard 2009). These observations support the view that at least some luminous LBV stars are the end point of the evolution and not a transition phase. This view

is however still in contradiction to certain current stellar evolution models (Meynet et al. 2011).

LBVs span quite a large range of magnitudes and variability types (Humphreys & Davidson 1994). Some of them show “normal eruptions” also called an S Dor variability phase. During this phase the star may brighten by up to two magnitudes in the visual, but the bolometric luminosity remains essentially constant. Other LBVs occasionally experience “giant eruptions”, during which they increase their luminosity and can reach $M \approx -14^m$ (4–6 mag brighter than their typical quiescence magnitudes). Among the 35 Galactic LBVs (confirmed and candidate) (Clark et al. 2005) only three (η Car, P Cyg and AFGL2298) were observed during giant eruptions (Humphreys & Davidson 1994; Clark et al. 2009). Several examples of eruptions accompanied with changes in bolometric luminosity have been studied spectrally (such as HD5980 (Koenigsberger 2004), NGC 2363-V1 (Drissen et al. 2001), AFGL2298 (Clark et al. 2009)). These giant eruptions are not only spectacular events but are probably responsible for bulk of the mass loss by very massive stars (Smith & Owocki 2006).

Observations of Galactic LBV stars are inevitably connected with difficulties in determination of the distance and interstellar extinction, that results in huge uncertainties in their bolometric luminosities. Hence studying these rare objects in nearby galaxies is potentially more prospective, though extragalactic objects are more distant and in this sense more difficult targets for spectral observations.

[★] Based in part on data collected at Subaru Telescope and obtained from the SMOKA, which is operated by the Astronomy Data Center, National Astronomical Observatory of Japan, while other data were taken from the archive of Special Astrophysical Observatory (SAO) of Russian Academy of Sciences (RAS)
[†] E-mail: olga.maryeva@gmail.com

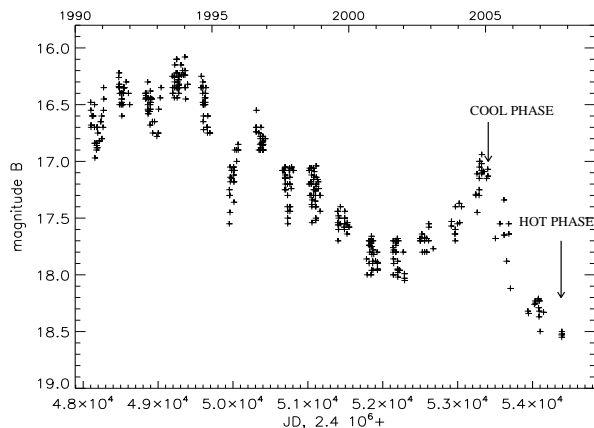


Figure 1. B-band light curve of V532. Arrows indicate the dates of spectral observations.

Romano's star is located in the outer spiral arm of the M33 galaxy at a distance of about $17'$ from the centre. The first light curve for V532 was presented by Romano (1978), while the first spectral observations were obtained in 1992 (Szeifert 1996). As it demonstrates pronounced photometrical and spectral variability (Kurtev et al. 2001; Polcaro et al. 2003), V532 is classified as an LBV. The object changes from a B emission line supergiant in the optical maximum (Szeifert 1996), through Ofpe/WN (WN10, WN11) and WN9 toward a WN8-like spectrum in deep minima (Maryeva & Abolmasov 2010). Figure 1 shows a B-band light curve of V532 from 1990 to 2008.

In 2004-2005, V532 becomes brighter by about 1^m in B and reaches 17^m in this band (see Zharova et al. (2010), Maryeva & Abolmasov (2010), and Polcaro et al. (2010) for details). We classify the spectra obtained during this period as WN11, in agreement with the estimates by Polcaro et al. (2010). Starting from the middle 2005, Romano's star weakens in all bands. Its visible magnitude reaches $18^m.68$ in the V band in February 2008. Recently, it exhibits a slight brightening by about $0^m.2$ (Polcaro et al. 2010). The spectral class in early 2008 is estimated by us as WN8 (Maryeva & Abolmasov 2010).

In this work we investigate the optical spectra of V532 in two different states, the brightness minimum of 2008 and a moderate brightening in 2005, using the non-LTE radiative transfer code CMFGEN (Hillier & Miller 1998). Below, we will refer to these two states as to the hot and cool phases, respectively.

This paper is organized as follows. Observational data and data reduction process are described in Section 2. In Section 3 we describe the basic properties of the CMFGEN code. We devote Section 3.2 to characteristic diagrams, while in Section 3.3 and Section 3.4 we present and analyse the modeling results for hot and cool phases of V532. In Section 4 we discuss the results. Finally, Section 5 we summarize the main points of our work.

2 OBSERVATIONS AND DATA REDUCTION

In this work, we use one spectrum of Romano's star obtained during the outburst in 2005 at the Special Astrophysical Observatory (SAO) 6m telescope ¹. For studying Romano's star at minimum brightness we use one spectrum obtained in January 2008 at the 6m SAO telescope and one spectrum obtained at the SUBARU telescope ². The 6m telescope data were obtained with the SCORPIO multi-mode focal reducer in the long-slit mode (Afanasiev & Moiseev 2005). One exposure 1200 s in length was obtained with the SUBARU telescope with the Faint Object Camera (FOCAS) (Kashikawa et al. 2002) in October 2007. VPHG450 grism was used providing the spectral range of 3750-5250 Å. Slit width of $0''.5$ implies spectral resolution of about 1.7 Å . Observational log information on the data used in this work is summarized in Table 1.

All the SCORPIO spectra were reduced using the *ScoRe* package. *ScoRe* was written by Maryeva and Abolmasov in IDL language for SCORPIO long-slit data reduction. This package consists of procedures written by V.Afanasiev, A.Moiseev, P.Abolmasov and O.Maryeva. Package includes all the standard stages of long-slit data reduction process. FOCAS data were reduced in IDL development environment using procedures similar to those consisting *ScoRe* but taking into account the specific features of FOCAS. We describe the observational data and data reduction process in more detail in Maryeva & Abolmasov (2010).

3 THE MODEL

3.1 CMFGEN Code

For our analysis we used the non-LTE radiative transfer code CMFGEN (Hillier & Miller 1998). CMFGEN has been applied to several classes of objects where non-LTE effects and stellar wind are important (e.g., WR, LBV, and O stars). More recently, CMFGEN was used to investigate the photospheric phase of Type II supernovae (Dessart & Hillier 2005). CMFGEN solves radiative transfer equation for objects with spherically-symmetric extended outflows using either the Sobolev approximation or the full comoving-frame solution of the radiative transfer equation. To facilitate simultaneous solution of the transfer equation and statistical equilibrium equations, partial linearization method is used. To facilitate the inclusion of metal line blanketing in CMFGEN, superlevel approach (Anderson 1989, 1991) is used. In this formalism, levels with similar properties are treated as one and have identical departure coefficients. This allows to save a considerable amount of computer memory and time. Recent versions of the code incorporate also the effect of level dissolution, influence of resonances on the photoionization cross section, and the effect of Auger ionization.

Clumping is incorporated into CMFGEN using volume

¹ Spectral data were taken from the archive of Special Astrophysical Observatory (SAO) of Russian Academy of Sciences (RAS) (<http://www.sao.ru>)

² Spectral data from the SUBARU telescope were taken from the SMOKA science archive (Baba et al. 2002) (<http://smoka.nao.ac.jp>)

Table 1. Observational log for the spectral data used in the work. S/N is signal-to-noise ratio per resolution element.

Date		Exposure time [s]	Grism	Spectral range [Å]	$\delta\lambda$ [Å]	S/N	Seeing ['']	Spectral standard star
06.02.2005	SCORPIO	2×300	VPHG550G	3700-7200	10	8	1.7	G248
08.01.2008	SCORPIO	2×900	VPHG1200R	5700-7500	5	20	2.1	BD25d4655
08.10.2007	FOCAS	1200	VPHG450	3750-5250	1.7	30	0.53	BD40d4032

filling factor approach (Hillier & Miller 1999). Filling factor is allowed to depend on radius. By default, the wind is considered homogeneous at the hydrostatic radius and becomes more and more clumped with the wind velocity. Taking clumping into account decreases the derived mass loss rates by a factor of $\sim 3 - 5$. The unclumped and clumped mass loss rates are related to the volume filling factor f as $\dot{M}_{uncl} = \dot{M}_{cl}/\sqrt{f}$.

Each model is defined by the hydrostatic stellar radius R_* , luminosity L_* , mass-loss rate \dot{M}_{cl} , filling factor f , wind terminal velocity v_∞ , stellar mass M , and by the abundances Z_i of included species. Hydrodynamic equations are not solved for, instead we propose β -law for velocity and fix mass loss rate for every model. This allows to define the density structure throughout the wind.

3.2 Diagnostic Diagrams

In order to reproduce the spectrum of V532 obtained in October 2007 while the object was in a deep minimum we took the model of the WN8 star WR40 (HD96548) calculated by Herald et al. (2001) and gradually changed the parameters of the model. We calculated a grid of about 130 models with different parameter values (luminosity, mass-loss rate, mass, elementary abundances). Luminosity was varied in the range $(0.4 - 2) \times 10^6 L_\odot$. For every model, we recalculated the model flux for the distance of M33. For our calculations we adopted a distance to M33 of $D = 847 \pm 60$ kpc, which gives a distance modulus of $(m - M) = 24.64 \pm 0.15^m$ (Galleti et al. 2004). Then, the simulated spectra were convolved with B- and V-band sensitivity filters. The resulting fluxes were converted to magnitudes (Leng 1974) and compared to the photometrical data ($B = 18^m.5 \pm 0.05$ and $V = 18^m.68 \pm 0.05$). According to the detailed dust maps of M33 by Hippelein et al. (2003) the effect of the intrinsic extinction should be negligible near the object. Extinction in the Galaxy is estimated as $E(B - V) = 0^m.052$ by the NED extinction calculator (Schlegel et al. 1998). This value is well inside the errors for the observed $B - V$ colour index but affects the observed luminosity values that should be thus increased by $\sim 0^m.17$.

Mass loss rate was varied in the limits $(1.2 - 7.7) \times 10^{-5} M_\odot \text{yr}^{-1}$ typical for WN8-WN11 stars (Crowther et al. 1995c; Hamann et al. 2006). In all the models we assume that the volume filling factor at infinity equals $f_\infty = 0.1$. Since V532 resides in low-metallicity environment, we considered only sub-solar iron abundances ($\text{Fe}/\text{Fe}_\odot = 0.4 \pm 0.15$). We also expected sub-solar abundances for Si, Mg, Na.

The velocity law used was assumed a simple β -law with $\beta = 1$. Photospheric velocity was set to 100 km/s and the terminal velocity is 400 km/s for all the models used for diagnostic diagrams. Below we investigate the effect of variations in β parameter and photospheric velocity on model spectra. Profile fitting for the triplet lines of He I (such as $\lambda 3889, 4025, 4471$) allows to estimate the terminal velocity as $\sim 400 \text{ km s}^{-1}$ (Maryeva & Abolmasov 2010).

Every model was classified using the equivalent width (EW) ratio of emission components of He I $\lambda 5876$ and He II $\lambda 5411$ (Smith, Shara & Moffat 1996). More precise estimates of physical conditions in the wind and atmosphere may be made using equivalent width ratios that weakly depend on spectral resolution and elementary abundances and also allow to exclude the contribution of a possible circumstellar nebula.

We construct several characteristic diagrams to compare the model spectra with the observations using equivalent width ratios. Figure 2 shows one such diagram. Modeling is complicated by the nebula surrounding V532. Therefore we use the characteristic EW ratios of He I $\lambda 4686$ to He I $\lambda 5876$ (these lines form both in the stellar atmosphere and in the nebula) and He II $\lambda 5411$ /He I $\lambda 4713$ (contribution of the nebula to these two lines should be negligibly small). In this diagram, models fall along a narrow curve with the spectral class changing smoothly along it. Effective temperature changes from $T_* \lesssim 25\text{kK}$ for the lower left corner toward $T_* \gtrsim 40\text{kK}$ for the upper right. Model distribution in a narrow locus along a single curve is probably connected to the correlated behavior of emission lines of He II as well as He I. Most models shown in the diagram have identical wind velocity and structure but different radii, luminosities and mass loss rates. We see that some real stars lie near this locus while WR 108 is offset. WR 108 is an unusual WN9 star — it has a higher terminal velocity ($\sim 1200\text{km/s}$, according to Hamann et al. (2006)) than other WN9 stars. Crowther et al. (1995a) classified WR 108 as intermediate star between normal Of and WN stars.

Bright hydrogen lines are present in the spectra, evidently stronger than in the spectra of ordinary late WN stars. In this sense, Romano's star is similar to H-rich WN stars. Therefore we calculate models with H/He = 0.75 – 2.6 (by number) that is typical for hydrogen WR stars. For the models that reasonably fit the observed equivalent widths, we varied the chemical composition and filling factor to fit the line strengths of individual elements and line profiles, correspondingly.

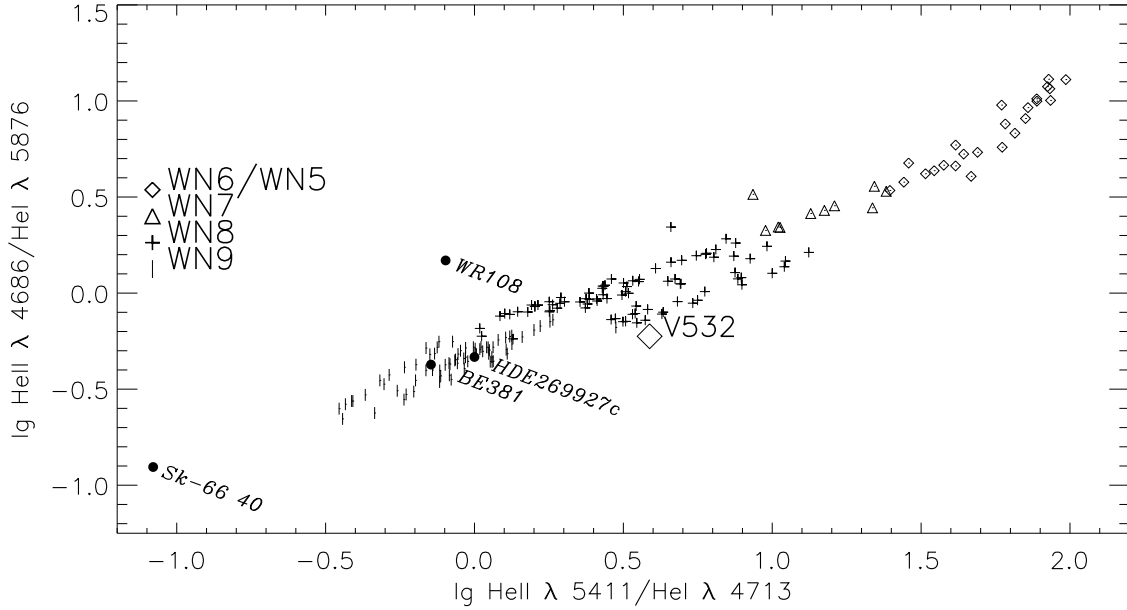


Figure 2. The plot of the EW ratio logarithm $\log(\text{He II } 4686 / \text{He I } 5876)$ versus $\log(\text{He II } 5411 / \text{He I } 4713)$. V532 location in October 2007 (hot phase) is marked by a diamond. Sk-66 40 (WN10), BE381 (WN9), HDE269927c (WN9) and WR108 (WN9-abs) are shown for comparison. Data on these objects were taken from Crowther et al. (1995b).

3.3 Hot-Phase Spectrum

In Figure 3 we show the observed spectra of V532 at minimum brightness and the best-fit model spectrum. Figure 3 shows good agreement between the observed and model spectra. Both in observational data and in the best-fit model, singlet and triplet lines of He I show different profile shapes: triplet lines have typical P Cyg profiles while singlets are pure flat-topped emissions.

For this model, the best-fit volume filling factor at infinity $f_\infty = 0.1$, mass loss rate $\dot{M}_{cl} = 1.9 \times 10^{-5} \text{M}_\odot \text{yr}^{-1}$ (that corresponds to unclumped $\dot{M}_{uncl} \simeq 6 \times 10^{-5} \text{M}_\odot \text{yr}^{-1}$). The stellar temperature T_* follows from the relation $L_* = 4\pi R_*^2 \sigma T_*^4$, and the effective temperature at the photosphere T_{eff} is defined by the Rosseland optical depth of 2/3. The values obtained for T_* , T_{eff} and other physical parameters are listed in Tables 2 and 4. Errors in luminosity given in the table are determined by the uncertainties of the photometrical data. The errors in the H/He ratio are from the model fitting only.

Surface chemical abundances obtained for V532 are listed in Table 3. Abundance pattern is consistent with the moderately sub-solar metallicity of M33 ($[\text{Fe}/\text{H}] \sim -0.5$), but nitrogen is significantly over-abundant (~ 6.4 solar). The latter value is consistent with the existing evolutionary models and with the data on other nitrogen-rich WR stars (Herald et al. 2001). Silicon abundance was adjusted using Si III $\lambda 4565.05$ and Si IV $\lambda \lambda 4088.90, 4116.10$ lines, magnesium abundance using Mg II $\lambda 4481.13$. Ne, Al, S, Ar and Ca abundances were fixed relative to He because they are poorly constrained by observational data due to the lack of strong lines for these elements. We assume these abundances identical to those for WR40.

After we obtained a model reasonably approximating

Table 3. Derived stellar abundances for Romano’s star. Abundances for all the elements are identical for the two phases within the uncertainties.

SPECIES	Number Fraction	Mass Fraction	Z_i/Z_\odot
H	1.9	3.18×10^{-1}	0.45
He	1.0	6.7×10^{-1}	2.4
C	1.0×10^{-4}	2×10^{-4}	0.07
N	3.0×10^{-3}	7×10^{-3}	6.4
O	8.0×10^{-4}	2.2×10^{-3}	0.23
Ne	2.4×10^{-4}	8.1×10^{-4}	0.47
Na	7.0×10^{-6}	2.7×10^{-5}	0.78
Mg	5.0×10^{-5}	2×10^{-4}	0.31
Al	8.4×10^{-6}	3.8×10^{-5}	0.7
Si	2.0×10^{-4}	1.0×10^{-3}	1.43
S	2.3×10^{-5}	1.2×10^{-4}	0.34
Ar	6.5×10^{-6}	4.4×10^{-5}	0.43
Ca	4.2×10^{-6}	2.8×10^{-5}	0.44
Fe	4.87×10^{-5}	4.6×10^{-4}	0.34

the observed spectra and consistent with the photometrical data we investigated the effects of photospheric velocity on the model spectrum and the derived model parameters. Decrease in photospheric velocity implies increase in Rosseland optical depth that affects both T_{eff} and $R_{2/3}$. These changes practically do not affect hydrogen and neutral helium lines, while the EW of the He II $\lambda 4686$ emission increases by about 14% when photospheric velocity decreases by a factor of two. Table 2 gives the parameters of a model with $v_{phot} = 10 \text{ km s}^{-1}$ that reproduces the spectrum indistinguishable from the current best-fit model with $v_{phot} = 100 \text{ km s}^{-1}$. One order of magnitude uncertainty in

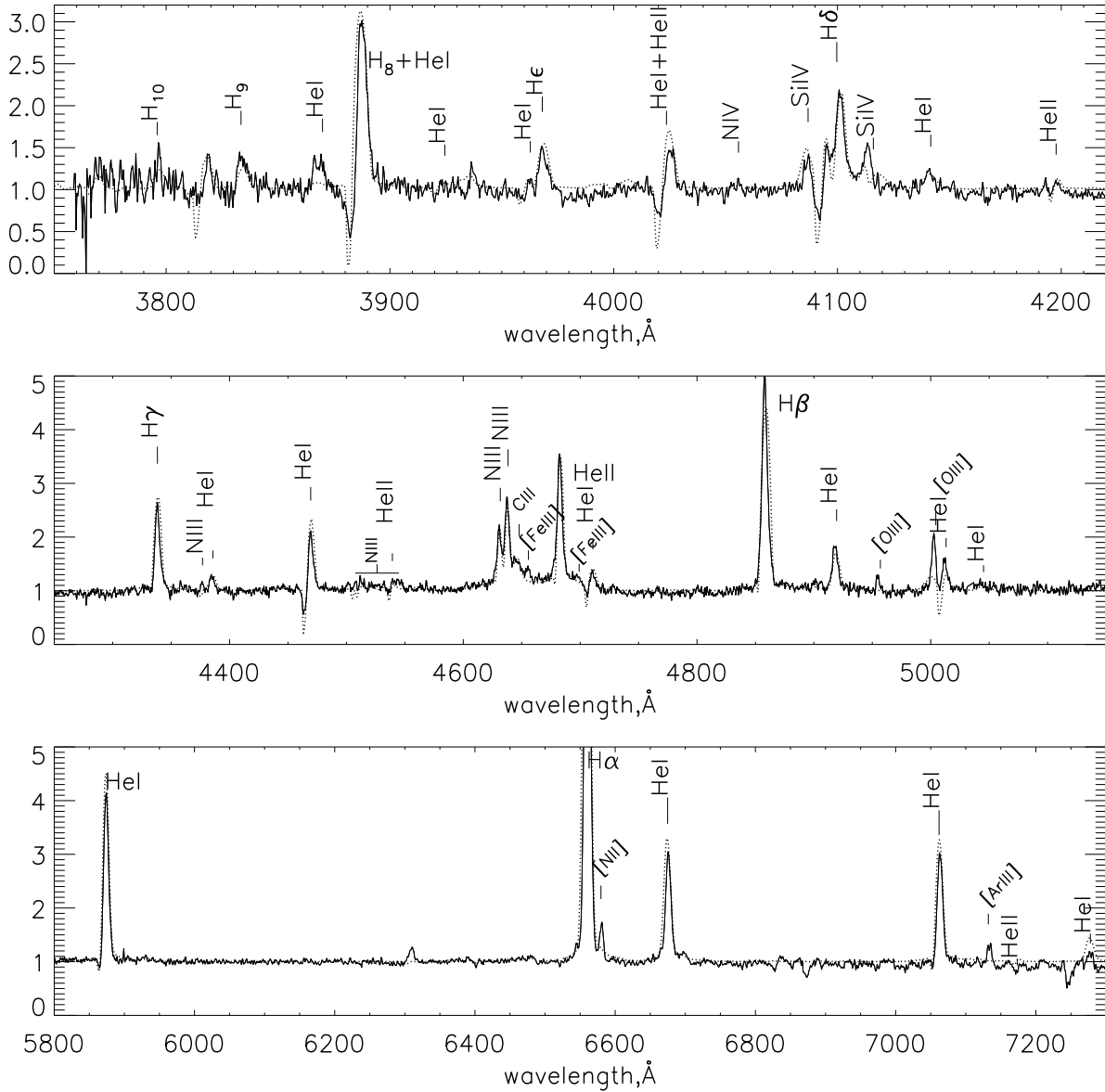


Figure 3. Normalized hot-phase optical spectra compared with the best-fit CMFGEN model (dotted line). Bottom panel shows the spectrum obtained with SCORPIO, top and middle panels show the spectrum obtained with FOCAS. The model spectrum on bottom panel is convolved with the 5Å-wide Gaussian instrumental profile.

Table 2. Best-fit model parameters for different values of β and photospheric velocity. H/He denotes hydrogen number fraction relative to helium.

β	V_{phot} [km/s]	V_{∞} [km/s]	T_* [kK]	R_* [R $_{\odot}$]	T_{eff} [kK]	$R_{2/3}$ [R $_{\odot}$]	L_* [10 $^5 L_{\odot}$]	\dot{M}_{cl} [10 $^{-5} M_{\odot} \text{ yr}^{-1}$]	H/He
1	100	400	34.0 \pm 0.5	20.8 \pm 1.	31.7 \pm 0.5	23.9 \pm 0.7	5.2 \pm 0.2	1.9 \pm 0.2	1.9 \pm 0.2
1	10	400	33.0 \pm 1.0	21.6 \pm 1.2	29.4 \pm 0.5	27.3 \pm 2.0	5.0 \pm 0.25	1.6 \pm 0.1	1.9 \pm 0.2
4	100	500	33.0 \pm 1.0	21.6 \pm 1.2	29.0 \pm 1.0	27.8 \pm 2.0	5.0 \pm 0.25	1.6 \pm 0.15	2.0 \pm 0.2

photospheric velocity results in 3% and 10% uncertainties in luminosity and mass loss rate, respectively.

3.3.1 Hot-Phase Spectrum with $\beta > 1$

As stated above the velocity law used was assumed a simple β -law:

$$v(r) \simeq v_{\infty} \left(1 - \frac{r_0}{r}\right)^{\beta},$$

with

$$r_0 = R_* \left\{ 1 - \left(\frac{v_{phot}}{v_{\infty}} \right)^{1/\beta} \right\}$$

where v_{phot} is photospheric velocity. Above we fixed the β parameter to unity. In some objects in certain phases, however, β is known to become significantly higher, up to $\beta \sim 4$ (Najarro et al. 1997; Groh et al. 2009). In general, LBV stars have low $\beta \lesssim 1$ during optical minima, but the velocity law changes during eruptions (Guo & Li 2007). Let us now consider the effect of variable β parameter on model spectrum.

Figure 4 illustrates the dependence of the 4630-4713 Å blend shape on β . Increasing β produces higher equivalent widths of all the detectable lines of the blend. Besides, the wings of He II λ 4686 (see also section 4.2) become stronger. As a result, intensities of C III $\lambda\lambda$ 4647.4, 4650.3, 4651.5 lines change, while the line ratios of C III $\lambda\lambda$ 4647.4, 4650.3, 4651.5 remain more or less constant. For large β ($\beta \geq 2$) C III λ 4647.4 is stronger than other carbon lines, and the shape of the 4630-4713 Å blend changes. Intensity ratios of the carbon lines observed in the spectrum of V532 (see the right panel of Figure 4) argue for $\beta \simeq 4$. Increase of β affects the model spectrum similarly to increase in the mass loss rate. Therefore we may describe the observed spectrum by a model with $\beta = 4$ and a lower (by about 10%) mass loss rate.

Figure 5 shows comparison between the observed spectrum of Romano's star and the model with $\beta = 4$. The model with $\beta = 4$ fits better the triplet lines of helium, while He II λ 4686 is brighter than for the best-fit model with $\beta = 1$. Table 2 shows the best-fit parameters for the models with different values of photospheric velocity V_{phot} and β .

3.4 Cool-Phase Spectrum

In 2004-2005, V532 becomes brighter by about 1^m in B and reaches 17^m in this band. Colour index $B - V$ is constant within the observational errors ($B - V = -0^m.11$ for October 2007 and $-0^m.17$ for February 2005). Spectra obtained during this brightening we classify as WN11, in agreement with the estimates by Polcaro et al. (2010). To study Romano's star in the cool phase we use the spectrum obtained in February 2005 at the 6m SAO telescope.

Using the hot model as initial, we increased the mass loss rate and hydrostatic radius thereby decreasing the effective temperature. After obtaining a model consistent with the photometrical data ($V = 17^m.27 \pm 0.03$, $B = 17^m.1 \pm 0.03$, assuming $A_v = 0^m.17$) we began to vary the wind velocity and volume filling factor. The equivalent width of H α increases by 30% when f_{∞} is increased from 0.1 to 0.5. But the effective temperature at the photosphere and the photosphere radius vary insignificantly. Mass loss increase leads to

H α EW increase as well. A 18% variation of mass loss rate leads to approximately 18% variation in the EW value. But it also leads to significant changes in effective temperature and photosphere radius. Therefore we fixed \dot{M} and changed only f_{∞} . To compare the model spectrum with the observations we convolved the observed spectrum with the 10 Å-wide Gaussian instrumental profile. Figures 6 and 7 show the observed spectrum and the best-fit model spectrum convolved with the instrumental profile. The figures also show comparison between the raw (high-resolution) best-fit model spectrum and a spectrum of the LBV star P Cyg (B1Ia⁺) obtained in August 1998 and taken from *Elodie* archive (<http://atlas.obs-hp.fr/elodie/intro.html>). The spectra are unexpectedly similar.

For the best-fit model in the cool phase, volume filling factor at infinity $f_{\infty} = 0.5$. This value is factor of 5 higher than the one typically found for WR stars (Herald et al. 2001). Note that this value is equal to that for P Cyg (Najarro 2001), thus confirming the similarity of these objects. Filling-factor seems to depend strongly on the mass loss rate or on the spectral state, changing from ~ 0.1 for late WN stars to ~ 0.5 for B-type hypergiants. Self-consistent modeling of wind acceleration is needed to understand the mechanisms leading to the strong clumpiness of the winds of Wolf-Rayet stars.

Mass loss rate for this model is $\dot{M}_{cl} = (4.5 \pm 0.2) \times 10^{-5} M_{\odot} \text{yr}^{-1}$, luminosity is $(7.7 \pm 0.25) \times 10^5 L_{\odot}$, $T_{eff} = 20.4 \pm 1.0$ kK. Wind and stellar parameters of V532 in the maximum of brightness are given in Table 4. Surface chemical abundances are the same as for the hot-phase model (see Table 3).

4 DISCUSSION

4.1 Evolution of the Physical Parameters

We model the spectra of V532 in maximum of brightness ($V=17^m$, Feb. 2005) and in minimum of brightness ($V=18^m.6$, Oct. 2005) using the non-LTE radiative transfer code CMFGEN. Stellar parameters derived for both hot- and cool-phase models are given in Table 4. For comparison, the values of these parameters for some other WN stars taken from the literature are given in the table. Note that the parameters of the Galactic WN8 stars WR124, WR16 and WR40, as well as the LBV AG Car in photometric minima and LBV P Cyg were calculated using CMFGEN models taking clumping into account (see Crowther et al. (1999); Herald et al. (2001); Groh et al. (2009); Najarro (2001)). On the other hand modeling of the WN9h stars R84 and BE381 did not account for clumping, and that may lead to mass loss rate overestimates. Table 4 shows that V532 in minimum of brightness is similar to a classical WN8 star, but the wind velocity is lower, characteristic rather for a WN9 star. We see that relative hydrogen abundance (H/He) for V532 is similar to that of WN8h stars given in the table. V532 as well as other LBVs AG Car and P Cyg (Groh et al. (2009); Najarro (2001)) has significantly enhancement of helium (more than a factor of 2 relative to solar), that would correspond to the end of hydrogen shell-burning phase. High nitrogen content and depletion of carbon and oxygen are indicative of material which has undergone the CNO cycle.

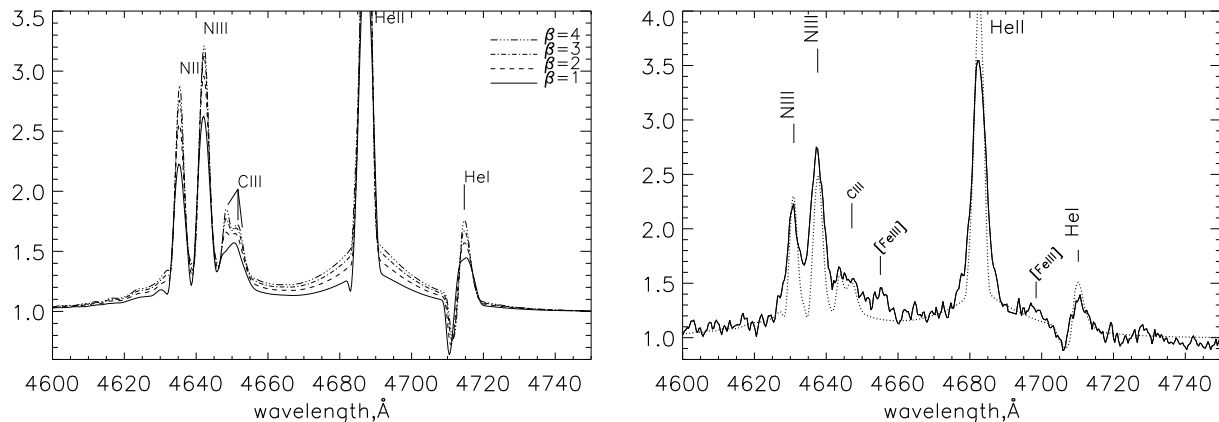


Figure 4. Left panel: effects of parameter β on the profile of 4630-4713 Å blend. Right panel: fitting of the 4630-4713 Å blend. Observational spectrum is shown by a solid line, dotted line is our hot-phase model calculated with CMFGEN ($\beta = 4$).

Our results agree with the contemporary understanding of V532 and Galactic LBV stars as a transitional stage from main-sequence supergiants to WR stars.

In February 2005, during the outburst, parameters of the star correspond to the spectral class WN11. The model spectrum is similar to the spectrum of P Cyg. V532 shows a WN11 spectrum in the maximum, while the classical LBVs like AG Car and P Cyg become WN11 only in the deep minima and in the long-lasting quiet state, respectively. Note however that V532 had a strong maximum in 1993 ($0^m.9$ brighter than in February 2005) and exhibited a B-supergiant spectrum. Hence, V532 shows stronger spectral variability than AG Car.

The two phases, hot and cool, are mainly distinguished by the photosphere radius, that is about three times larger in the cool phase. Three basic parameters vary simultaneously and make measurable contributions to the observed inflation of the star. For the two states, \dot{M} differ by a factor 2.4, and the wind velocity is 1.8 times larger for the hot state. It is easy to check that the size of the wind photosphere should scale approximately as:

$$R_{ph} \propto \left(\frac{M_{\odot}}{v_{\infty}} \right)^n,$$

where $n = 1$ in the case of pure scattering wind (mass-absorption coefficient $\kappa = \text{const}$) and $n = 2/3$ when $\kappa \propto \rho$, as for true absorption processes. Hence, R_{ph} is expected to vary by a factor 3 to 5, in consistence with the observed value of 2.9. Our model favours correlation of hydrostatic radius with mass loss rate.

Romano's star is situated near a young OB-association OB 89. Probably V532 was a member of OB 89 and was ejected via slingshot-type dynamical interaction. In more detail we consider this suggestion in Maryeva & Abolmasov (2011).

Polcaro et al. (2010) presented the values of bolometric luminosity, effective temperature and radius of Romano's star, using bolometric corrections for known WN8 and WN11 stars. Here, we use a more comprehensive way to estimate the bolometric luminosity. But the main conclusion

holds: bolometric luminosities of V532 were different in 2005 and 2008. The luminosity of V532 in 2005 ($L_* = 7.7 \cdot 10^5 L_{\odot}$) is 1.5 times higher. Therefore, V532 should be considered one more LBV (after the objects mentioned by Koenigsberger (2004); Drissen et al. (2001); Clark et al. (2009)) that changes its luminosity during (even moderate amplitude) eruption. In this sense, V532 behaves similarly to AG Car that has bolometric luminosity variations during its S Dor cycle (Groh et al. 2009).

4.2 The Broad Wings of the He II $\lambda 4686$ Emission

Polcaro et al. (2010) detect a broad ($\sim 1000 \text{ km s}^{-1}$) component of the He II $\lambda 4686$ line in the spectrum of V532 obtained in December 2008. Authors explain this component by a bimodal stellar wind. Although CMFGEN adopts spherical symmetry, the model profiles of this emission line possess similar, and sometimes even broader and brighter wings (Fig. 8). Observed wings may be explained by a more common phenomenon – by electron scattering. Strong and very broad emission wings were first found for LBVs in P Cygni by Bernat & Lambert (1978). Balmer lines in the spectrum of AG Car do have such wings, which extend to more than $\pm 1500 \text{ km s}^{-1}$ from the core of the line (Stahl et al. 2001). For P Cyg, electron scattering wings were reproduced by Najarro et al. (1997) in spherical symmetry. The wings are explained by scattering of line photons by free electrons of the stellar wind. Large widths of the wings reflect high thermal velocities of free electrons and does not correspond to bulk motion of the gas.

5 CONCLUSIONS

Using comoving frame numerical radiative transfer with the CMFGEN code, we estimate the physical parameters of the photosphere of Romano's star coming to the two principal conclusions. Firstly, in this object, variability is caused by correlated changes in mass loss rate, wind velocity and hydrostatic radius. Elementary abundances do not change significantly, in both states we find similar helium and nitrogen

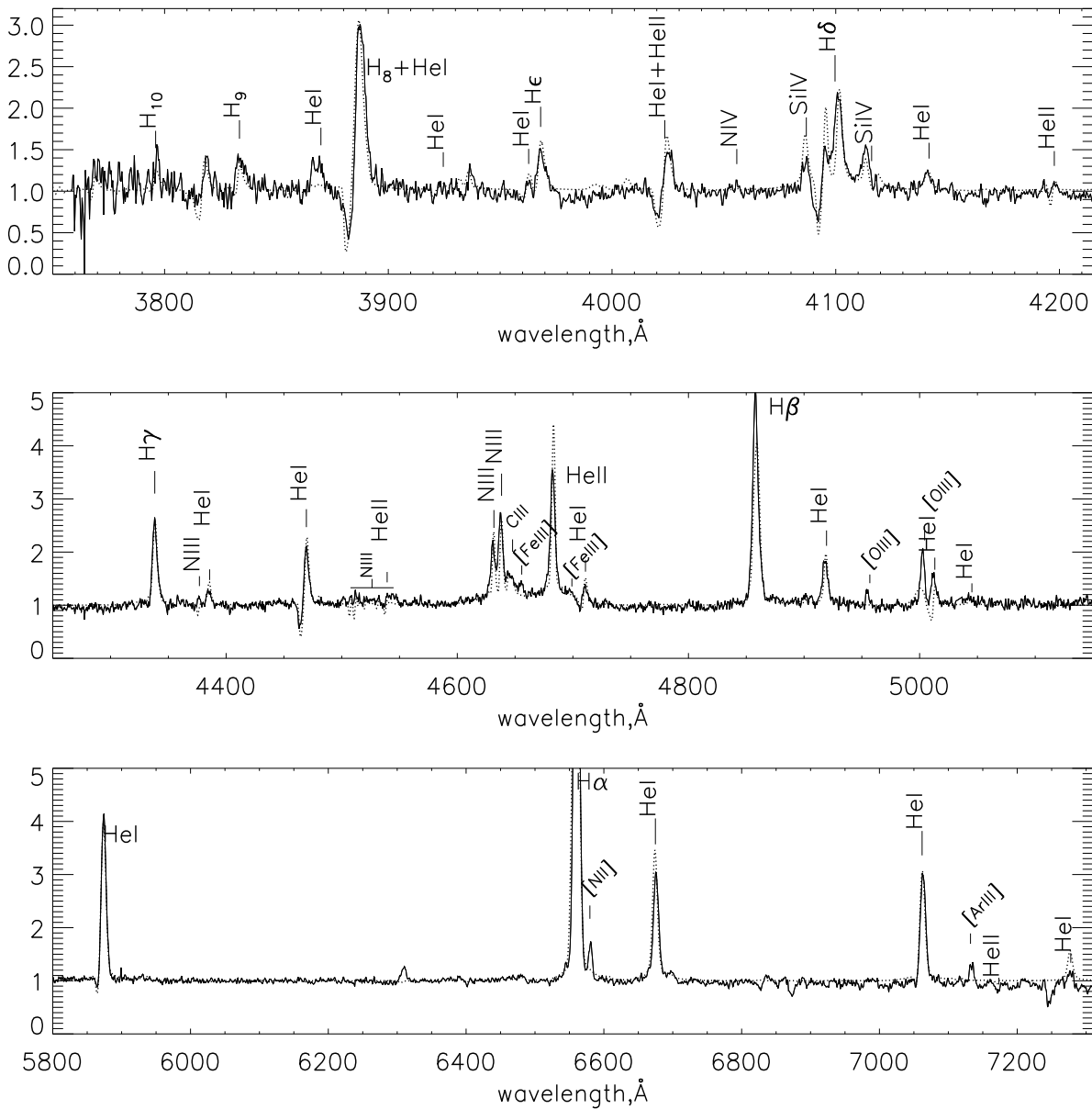


Figure 5. The normalized hot-phase optical spectra compared to a CMFGEN model with $\beta = 4$ (dotted line). Bottom panel shows the spectrum obtained with SCORPIO, top and middle panels show the spectrum obtained with FOCAS. The model spectrum on the bottom panel is convolved with the 5Å-wide Gaussian instrumental profile.

overabundance characteristic for hydrogen-rich WNL stars, $\text{H}/\text{He} \simeq 1.7 - 2.0$ and $\text{N}/\text{He} \simeq (3 - 5) \times 10^{-3}$.

We find that the bolometric luminosity of this object was higher during the eruption in 2005 by a factor of ~ 1.5 , that makes V532 one more example of an LBV that changes its luminosity. Together with the moderate intensity outburst of AFGL2298, its behaviour indicates that even moderate amplitude LBV outbursts are accompanied by changes in bolometric luminosity.

ACKNOWLEDGMENTS

We would like to thank the anonymous referee for valuable comments. The paper is partially based on spectral data retrieved from the ELODIE archive at Observatoire de Haute-Provence (OHP). Based in part on data collected at Subaru Telescope, which is operated by the National Astronomical Observatory of Japan, and taken from the SMOKA, which is operated by the Astronomy Data Center, National Astronomical Observatory of Japan. We also use the data from the archive of the Special Astrophysical Observatory. We also wish to thank John D. Hillier for his great code CMFGEN, both comprehensive and user-friendly, that we applied

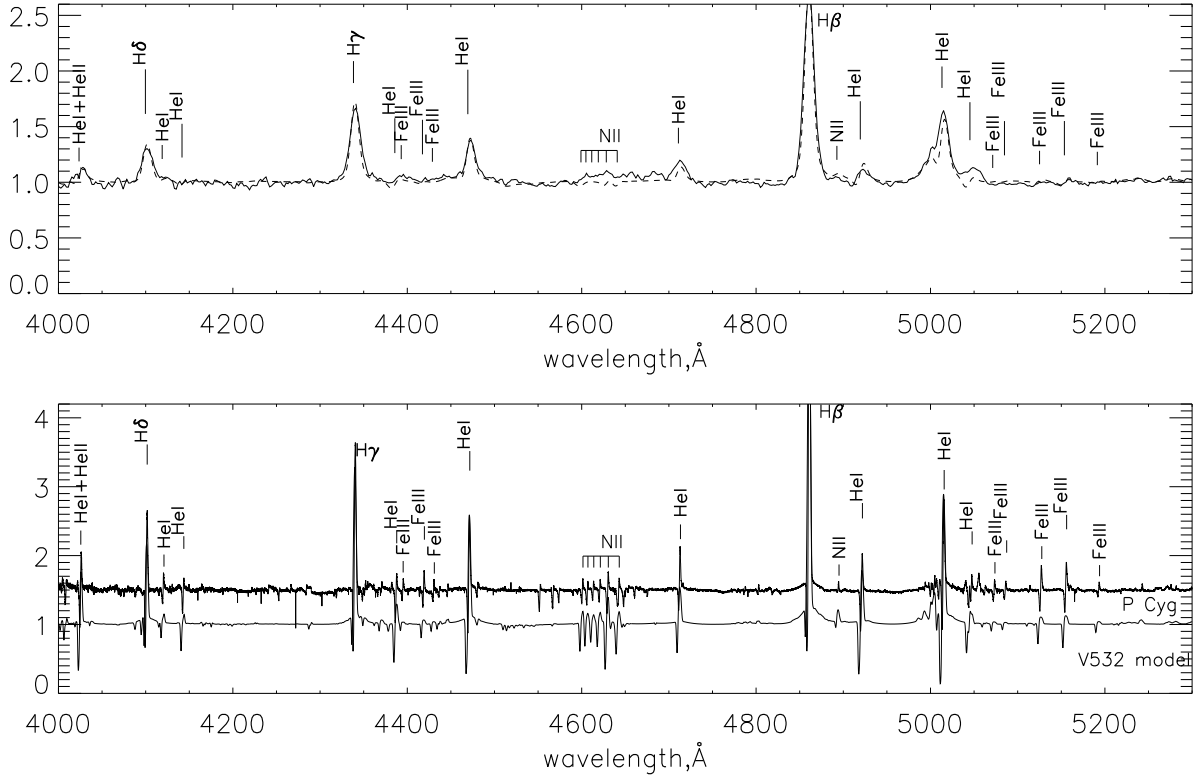


Figure 6. Fitting the cool-phase spectrum in the blue spectral range. Top panel: spectrum of V532 (Feb. 2005) (solid line) and our cool-phase model (convolved with the instrumental profile). Bottom: comparison of our cool-phase model spectrum with the archival spectra of the LBV star P Cyg. Spectra are normalized by the local continuum level.

Table 4. Derived properties of V532 in the maximum and the minimum of brightness, and comparison with related stars in M33, LMC and Milky Way (MW) galaxies, including the LBVs P Cyg and AG Car in visual minima (Dec 1990, Jul 2000).

Star	Gal.	Sp. type	T_* [kK]	R_* [R_\odot]	T_{eff} [kK]	$R_{2/3}$ [R_\odot]	$\log L_*$ [L_\odot]	$\log \dot{M}_{cl}$ [$M_\odot \text{ yr}^{-1}$]	f	v_∞ [km s $^{-1}$]	H/He	Ref
WR124	MW	WN8h	32.7	18.0			5.53	-4.7	0.1	710	0.7	[1]
WR40	MW	WN8h	45.0	10.6			5.61	-4.5	0.1	840	0.75	[2]
WR16	MW	WN8h	41.7	12.3			5.68	-4.8	0.1	650	1.2	[2]
R 84	LMC	WN9h	28.5	33.8	24.9	44.2	5.83	-4.40		400	2.5	[5]
BE 381	LMC	WN9h	30.6	20.8	27.5	26.0	5.54	-4.65		375	2.	[5]
AG Car Dec 1990	MW	WN11	24.64	67.4	21.5	88.5	6.17	-4.82	0.1	300	2.3	[4]
AG Car Jul 2002	MW	WN11	18.7	95.5	16.4	124.2	6.0	-4.33	0.25	195		[4]
P Cyg	MW	B1Ia $^{+}$			18.7	76.0	5.8	-4.63	0.5	185	2.5	[3]
V532 hot-phase	M33	WN8	34.0	20.8	31.7	23.9	5.7	-4.72	0.1	360*	1.9	
V532 cool-phase	M33	WN11	22.0	59.6	20.4	69.1	5.89	-4.4	0.5	200	1.4	

[1]- Crowther et al. (1999), [2]- Herald et al. (2001), [3]- Najarro (2001), [4]- Groh et al. (2009), [5] - Crowther & Smith (1997)

* - v_∞ was estimated using HeI lines (Maryeva & Abolmasov 2010)

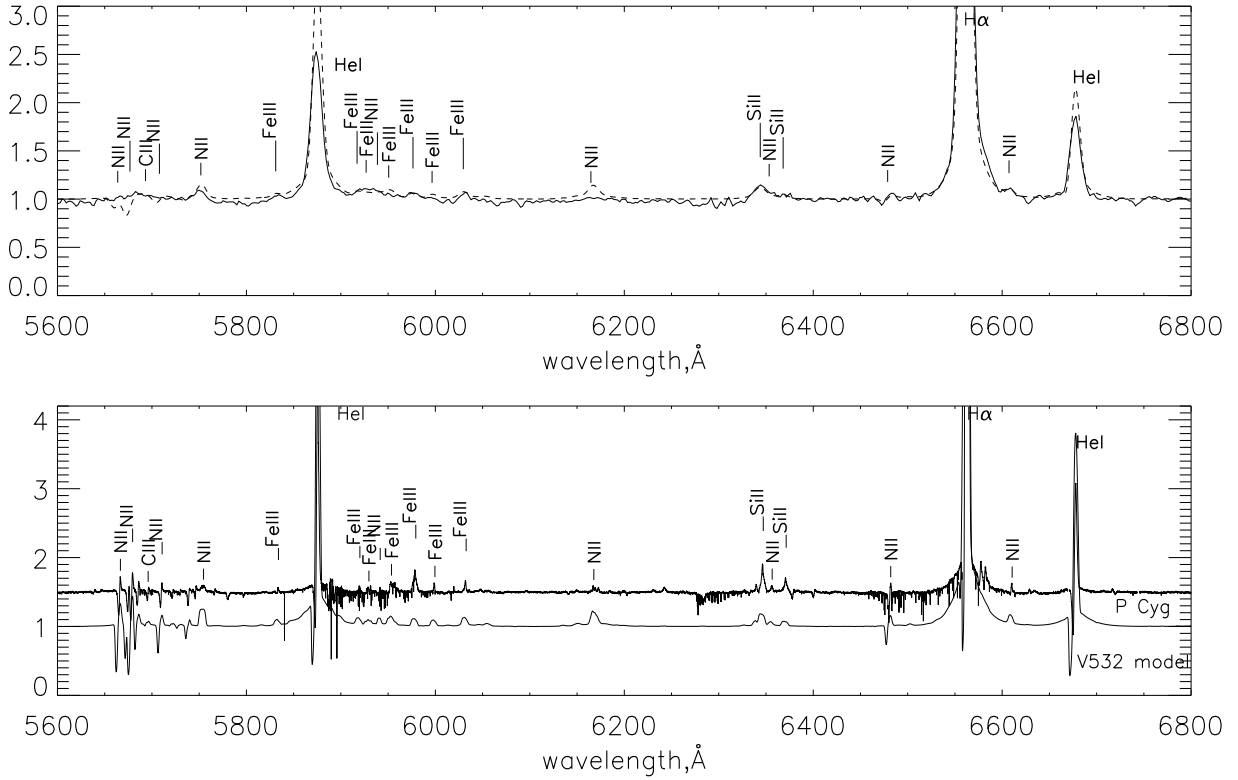


Figure 7. Fitting the cool-phase spectrum in the red spectral range. Top panel: Spectrum of V532 (Feb. 2005) (solid line) and our convolved cool-phase model. Bottom: comparison of our cool-phase model with observation spectrum of LBV star P Cyg. Spectra are normalized by the local continuum level.

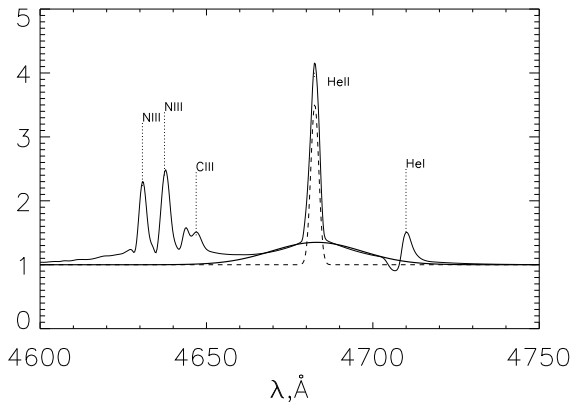


Figure 8. Approximation of the He II $\lambda 4686$ emission in the model spectrum by two Gaussians. The broad component of He II $\lambda 4686$ is shown by a thick line, narrow by a dashed line.

to fit and analyse the data. One of us (P. A.) thanks leading scientific schools grant NSH-7179.2010.2 for support.

REFERENCES

- Afanasiev V. & Moiseev A. 2005, *Astronomy Letters*, 31, 194
- Anderson L. 1991, in *Stellar Atmospheres: Beyond Classical Models*, ed. L. Crivellari, I. Hubeny, D.G. Hummer, NATO ASI Ser. C, Vol. 341 (Dordrecht: Kluwer), 29
- Anderson L.S. 1989, *ApJ*, 298, 848
- Baba H., Yasuda N., Ichikawa S., Yagi M., Iwamoto N., Takata T., et al. 2002, *ADASS XI*, eds. D. A. Bohlender, D. Durand, & T. H. Handley, ASP Conference Series, Vol. 281, 298
- Bernat A. P., Lambert D.L., 1978, *PASP*, 90, 520
- Clark J.S., Crowther P.A., Larionov V.M., Steele I.A., Ritchie B.W., Arkharov A.A., 2009, *A&A*, 507, 1555
- Clark J.S., Larionov V.M., Arkharov A. 2005, *A&A*, 435, 239
- Conti, P. S. 1984, in *IAU Symp. 105, Observational Tests of the Stellar Evolution Theory*, ed. A. Maeder & A. Renzini (Dordrecht: Kluwer), 233
- Crowther P.A., Hillier D.J., Smith L.J. 1995a, *A&A*, 293, 172
- Crowther P.A., Hillier D.J., Smith L.J. 1995b, *A&A*, 293, 403
- Crowther P.A. & Smith L.J., Hillier D.J., Schmutz W. 1995c, *A&A*, 293, 427
- Crowther P.A. & Smith L.J. 1997, *A&A*, 320, 500

- Crowther P.A., Pasquali A., De Marco O., Schmutz W., Hillier D.J., De Koter A. 1999, A&A, 350, 1007
- Dessart L., Hillier D.J. 2005 A&A, 439, 671
- Drissen L., Crowther P. A., Smith, L. J., Carmelle R., Roy, J.-R., Hillier D.J., 2001 ApJ, 546, 484
- Galletti, S., Bellazzini, M., Ferraro, F.R. 2004, A&A, 423, 925
- Gal-Yam Avishay, Leonard D. C. 2009, Nature, 458, 865
- Groh J.H., Hillier D.J., Damineli A., Whitelock P.A., Marang F., Rossi C. 2009, ApJ, 698, 1698
- Guo, J. H. & Li, Y., 2007, ApJ, 659, 1563
- Hamann W.-R., Gräfener G., Liermann A. 2006, A&A, 457, 1015
- Hippelein H., Haas M., Tuffs R.J., Lemke D., Stickel M., Klaas U., Volk H.J. 2003, A&A, 407, 137
- Humphreys R., Davidson K. 1994, PASP, 106, 1025
- Herald, J.E, Hillier D.J. Schulte-Ladbeck R.E. 2001, ApJ, 548, 932
- Hillier D.J., Miller D.L. 1998, ApJ, 496, 407
- Hillier D.J., Miller D.L. 1999, ApJ, 519, 354
- Kashikawa N., Aoki K., Asai R., Ebizuka N., Inata M., Iye M., et al. 2002, PASJ, 54, 819
- Koenigsberger G. 2004, Rev.Mex. AA, 40, 107
- Kurtev R., Sholukhova O., Borrisova J., Georgiev L. 2001, Rev.Mex. AA, 37, 57
- Leng K.R. 1974, Astrophysical Formulae Berlin – Heidelberg – New York: Springer-Verlag
- Maeder, A., & Meynet, G. 2000, ARA&A, 38, 143
- Maryeva O., Abolmasov P. 2010, Rev.Mex. AA, 46, 279
- Maryeva, O., Abolmasov, P. in preparation
- Meynet G., Georgy C., Hirschi R., Maeder A., Massey P., Przybilla N., Nieva M.-F. 2011, Bulletin de la Societe Royale des Sciences de Liege, 80, 266
- Najarro F. 2001, ASPC, 233, 133
- Najarro F., Hillier, D. J. & Stahl, O. 1997, A&A, 326, 1117
- Nota A., Livio M., Clampin M., & Schulte-Ladbeck R. 1995, ApJ, 448, 788
- Polcaro V.F., Rossi C., Viotti R.F., Gualandi R., Galletti S., Norci L. 2010, Astron.J, 411, 193
- Polcaro V.F., Gualandi R., Norci L. 2003, A&A, 411, 193
- Romano G. 1978, A&A, 67, 291
- Schlegel, D. J., Finkbeiner, D. P., & Davies, M. 1998, ApJ, 500, 525
- Stahl O., Jankovics, I., Kovacs, J., Wolf, B., et al. 2001, A&A, 375, 54
- Smith L.J., Crowther P.A., Prinja R.K. 1994, A&A, 281, 833
- Smith L.F., Shara M.M., Moffat F.J. 1996, MNRAS, 281, 163
- Smith, N., Gehrz, R. D., Hinz, P. M., et al. 2003, AJ, 125, 1458
- Smith N., Owocki, S. P. 2006, ApJ, 645, L45
- Smith, N., & McCray, R. 2007, ApJ, 671, L17
- Smith, N., Chornock, R., Li, W., Ganeshalingam, M., Silverman, J. M., Foley, R. J., Filippenko, A. V., Barth, A. J 2008, 686, 467
- Szeifert T. 1996, In: *Wolf-Rayet Stars in the Framework of Stellar Evolution* Eds. J.M.Vreux, A.Detal, D.Fraipont-Caro, E.Gosset and G.Rauw. 33rd Liege Institute Astroph. Coll., Liege, 459
- Weis K. 2001, Reviews in Modern Astronomy 14, ed.: Schielicke R.E., Springer-Verlag, 261, and astro-ph/104214
- Wolf B. 1989, Astronomy and Astrophysics, 217, 87
- Zharova A. V., Goranskij V. P., Fabrika S. N. & Sholukhova O. N., 2010, Perem. Zvezdy, accepted